Thin Solid Films, 220 (1992) 138–145

Physics and diagnostics of laser ablation plume propagation for high-T_c superconductor film growth

David B. Geohegan

Oak Ridge National Laboratory, P.O. Box 2008, Solid State Division, Oak Ridge, TN 37831-6056 (USA)

Abstract

The formation, composition and propagation of laser-produced plasmas used for pulsed laser deposition (PLD) of $Y_1Ba_2Cu_3O_{7-x}$ have been studied under film growth conditions. Four complementary spatially and temporally resolved *in situ* diagnostic techniques are applied to characterize the expansion of the laser plume into both vacuum and ambient gases: optical emission and absorption spectroscopy, fast ion probe measurements, and fast photography with a gated, image-intensified charge-coupled detector-array (ICCD) camera system. Transient optical absorption spectroscopy reveals large densities of ground state atoms, ions, and molecules in the plume as well as a slower component to the plume transport than is indicated by the plasma fluorescence and ion current.

Ablation into background gases results in scattering and attenuation of the laser plume. The exponential attenuation of the positive ion flux transmitted through 50–300 mTorr background oxygen is measured and used to define an overall ion–oxygen reaction cross-section $\sigma_{i-O_2} = 2.3 \times 10^{-16}$ cm^2 under the described film growth conditions.

The slowing of the laser plasma and formation of shock structures due to collisions with the ambient gas are described using ion probe measurements and ICCD photographic comparisons of expansion into vacuum and background oxygen. At the pressures used for PLD, distance–time $R-t$ plots derived from the photographs and ion probe waveforms indicate that the higher pressure plume initially expands through the ambient gas in accordance with a drag model (where $R = x_f[1 - \exp(-\beta t)]$), experiencing little slowing until a visible shock structure forms. Following a transition period, in which the plume appears to have two components, a single-component shock structure propagates in better agreement with a shock, or blast wave ($R = \xi_0(E/\rho_0)^{1/5}t^{2/5}$) model.

1. Introduction

The interaction of laser ablation plumes with background gases is currently receiving increased attention because of its importance to film growth by pulsed laser deposition (PLD) [1–8]. During PLD of yttrium barium copper oxide (YBCO) films, ambient oxygen scatters, attenuates and reacts with the ablation plume to form oxides and possibly clusters which may aid oxygen incorporation in the growing film [3, 5, 9]. During the trip from target to substrate, ablated atoms and ions from YBCO attain typical initial kinetic energies of about 40–70 eV within 1 mm of the target [2] and are then thermalized over a distance of several centimeters by collisions with 100–200 mTorr oxygen [7, 8].

As the amount of ablated material increases, such as for PLD or laser etching, gas dynamic effects are thought to play a leading role in determining the spatial and velocity distributions of the vaporized material. Collisions between the ejectants during the initial expansion are theorized to result in a Knudsen layer or unsteady adiabatic expansion zone which results in stopped or backward-moving material close to the pellet and strongly forward-peaked velocity distributions away from the pellet [10, 11].

Ablation into high pressure ambient gases results in shock waves and expansion fronts propagating through the backgrond gas [4–6, 10–15]. For PLD, ambient gas pressures must be kept low enough that some of the ablated species reach the substrate irrespective of the background gas shock wave. This complex problem, involving elements of both free expansion and shock wave propagation, is the subject of current experimental [4–6, 8–10, 12] and theoretical [11] activity.

In this paper, the transport of laser-ablated YBCO into vacuum and ambient oxygen is explored while reviewing four fast, *in situ* diagnostic techniques. The thermalization and attenuation of the propagating plasma are investigated with fast ion probes which detect the flux of positive ions transmitted through the gas. Fast photography with a gated, intensified charge-coupled detector-array (ICCD) camera is applied to provide two-dimensional images of the expansion of the visible plume for comparison with the ion probe and spectroscopic measurements. The results are compared with two models: a drag force model and a shock wave propagation model. The composition of the plume is temporally resolved by optical absorption and emission spectroscopy.

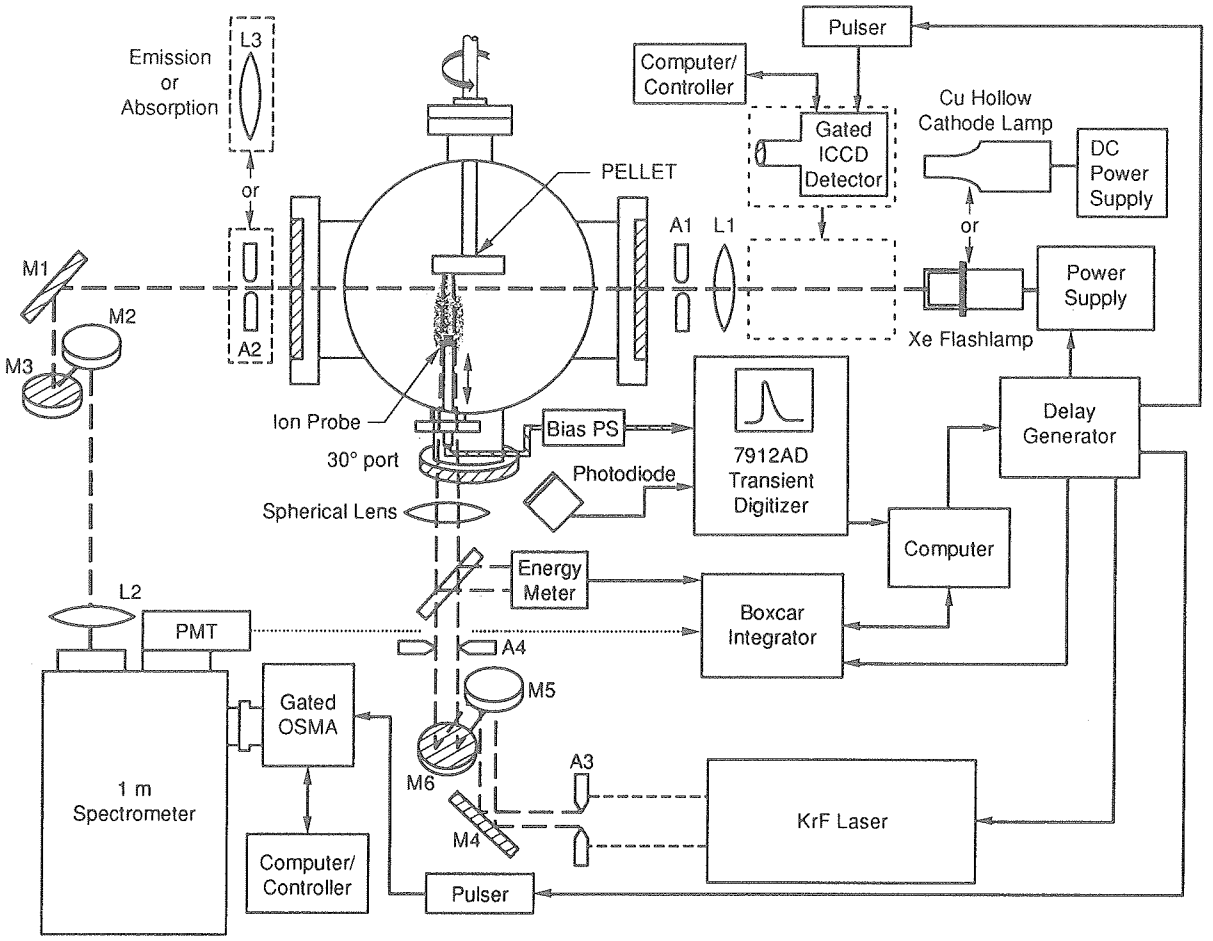

Fig. 1. Experimental apparatus used for optical absorption and emission spectroscopy, ion probe, and gated ICCD photographic measurements of laser-produced plasma plumes.

2. Experimental details

The experimental configuration for spatially and temporally resolved optical emission spectroscopy, optical absorption spectroscopy, ion probe measurements and fast ICCD photography is diagrammed in Fig. 1 and has been described before [7–9, 16, 17]. A high density $Y_1Ba_2Cu_3O_{7-x}$ pellet (W. R. Grace Co.) was rotated near the center of a 16 in diameter vacuum chamber. The central portion of a Lambda Physik EMG 210 excimer laser beam ($\lambda = 248$ nm, 30 ns full width at half-maximum pulse, 1 J pulse^{-1}) was apertured to typically about 1 cm^2 and focused by a single spherical or cylindrical lens to either a square or a line on the target surface at an incident angle of 30° from below.

Optical emission and absorption of the laser plume were spectrally resolved by a 1 m air path spectrometer with 2400 groove mm^{-1} grating, providing 0.04 Å resolution. The plume region was imaged onto the entrance slits of the spectrometer, sampling a vertical slice corresponding to about 50 μm of the horizontally expanding plume. In addition, a gated, intensified diode array (Princeton Instruments IRY-700RB) was utilized to record simultaneously plasma emission over 50 Å wide spectral regions with variable delays and adjustable gate widths above 3.8 ns. A fast (0.3 ns) photomultiplier provided temporal histories of a selected emission or absorption line to the transient digitizer for storage or the boxcar integrator for signal averaging during a spectral scan.

Optical absorption using the structured continuum from a pulsed xenon flashlamp and the dispersion of a 1 m spectrometer is observable as a result of the spectral broadening of the strong resonance lines of atoms and ions in the plume [16]. Alternatively, spectrally narrow, continuous wave hollow cathode lamps can be used in conjunction with a photomultiplier–interference filter system to capture the entire temporal history of a desired species.

A cylindrical copper Langmuir probe or, alternatively, a copper planar probe housed 2 mm behind a copper plane with 0.02 cm^2 aperture were both em-

ployed for measurements of the positive ion flux along the target normal. The ion probe was floated with respect to the chamber and pellet by terminating the coaxial signal line at the digitizer and by providing the bias with a completely isolated and shielded 1 μF capacitor bypassed 300 V battery and potentiometer in series with the 50 Ω signal line. The probes were operated at saturation in the electron-repelling regime with typically negative 100 V bias.

Fast, side-on views of the plume expansion were made by recording the overall visible emission from the plasma plume with a gated, ICCD camera system (Princeton Instruments ICCD-576G/RB). A 105 mm Nikon UV telephoto lens imaged a region extending 4.5 cm normal to the pellet, collecting light from throughout the plasma volume to form a weighted, two-dimensional image of the plume intensity. The detector utilizes a microchannel plate (MCP) which prevents photoelectrons from the photoemissive detector surface from reaching the phosphor–CCD array until a gate voltage pulse is applied. Fast (3.8 ns or longer) gate pulses (acting as the shutter for the camera) were supplied at variable times after the firing of the laser for "stop-action" images of the plume expansion. The MCP provides amplification and sensitivity beyond that of regular photography, allowing fainter images such as those found in the lower background gas pressures explored here to be captured.

It is important to note that the exposure chosen for the ICCD images is as difficult a problem as in ordinary photography. Overexposure loses detail in bright regions of interest while underexposure misses the fainter regions. For each exposure in these experiments, the gain on the MCP was set just short of saturation, to utilize the 14-bit dynamic range of each pixel on the 384×576 CCD array. The image was digitized and stored by a computer to be processed later with image-processing software.

3. Results and discussion

The ablation of $Y_1Ba_2Cu_3O_{7-x}$ into vacuum results in a highly forward-directed plume, with spatial deposits exhibiting $\cos^n\theta$ ($n > 4$) symmetry about the target normal [1]. At the high laser intensities ($I \approx 50$ MW cm^{-2}) used for PLD of YBCO, a bright plasma initiates at the pellet surface and expands with the brightest emission moving at $v \approx 1 \times 10^6$ cm μs^{-1} [2]. Fluorescence from excited states persists to long distances in conjunction with the ions and electrons in the plume, indicating a supersonic plasma pulse with collisional excitation kinetics at work in the high density regions. However, optical absorption spectroscopy by non-emitting ground state species reveals another, slower velocity component to the transport [9, 16].

Fast ICCD photography permits two-dimensional images of the visible plume expansion to be observed in vacuum [17], and these are given in Figs. 2(a)–2(f). The geometry for this experiment is diagrammed in the lower right-hand corner of Fig. 2. A rotating YBCO pellet is viewed side-on following irradiation by a 1.0 J cm^{-2} KrF laser pulse (2 mm $\times$ 2 mm square image on the pellet surface) incident at 30°. Fast 20 ns exposure times were used to freeze the motion of the plume (for $v = 1.0 \times 10^6$ cm s^{-1}, $v\Delta t = 0.2$ mm) in order to examine the spatial distribution of the fluorescence.

In vacuum, the plasma emission initiates on the surface of the pellet and then separates into two components. An essentially stationary component occupies a region out to $d \approx 1$ mm from the target surface and emits detectable light for $\Delta t \leqslant 2.0$ μs. A second component expands nearly one-dimensionally for the first 0.5 μs (Fig. 2(a)) and then expands freely in a highly forward-directed pattern with a constant leading edge velocity $v_{le} = 1.0$ cm μs^{-1}. This region of emission has been noted before [6, 9] and may result from gas collisions between the plume ejectants in the high pressure region of the initial expansion, resulting in a Knudsen layer with stopped and or backward-moving material [10, 11].

The $d < 1$ mm region was investigated by gated optical emission and absorption spectroscopy following 1 J cm^{-2} KrF irradiation, and time-resolved spectra from 596.7 nm $< \lambda <$ 601.4 nm are given in Fig. 3. The fluorescence temporal history shows excited states of yttrium, barium and weak emission from YO ($A^2\Pi$), all emitting detectable radiation until $\Delta t \approx 2.0$ μs (in agreement with Figs. 1(a)–1(c)). However, absorption of a xenon lamp continuum beam (width 0.5 mm) detects the same excited states of yttrium and barium, but also reveals the presence of large concentrations of ground state YO ($X\ ^2\Sigma$). This absorption lasts for several hundred microseconds (not shown), indicating the presence of a slow moving or stopped vapor. Optical absorption in other wavelength regions detects large densities of ground state neutrals, ions and molecules at late times and up to several centimeters from the target [16].

As background gas is introduced and the pressure is increased, several effects are evident.

(1) The fluorescence from all species increases as a result of increased collision rates on the leading edge of the expansion.

(2) Reactive scattering produces new gas phase species, such as the formation of YO from the ablation of yttrium into O_2 [1, 9].

(3) The plume boundary is slowed by collisions with the background gas.

(4) The amount of material penetrating the background gas is attenuated dramatically.

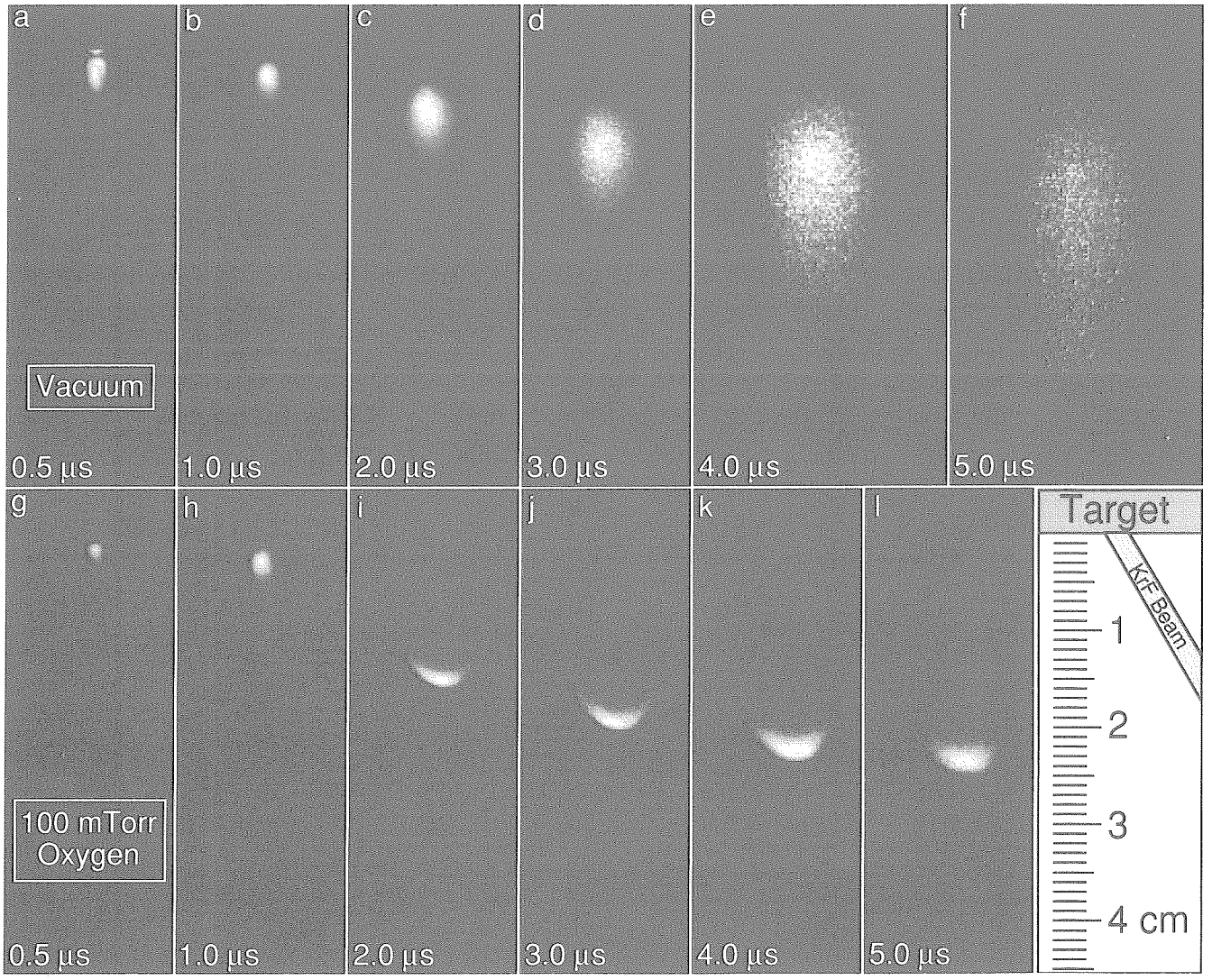

Fig. 2. ICCD photographs of the visible plasma emission (exposure times, 20 ns) following 1.0 J cm^{-2} KrF–YBCO ablation into (a)–(f) 1×10^{-6} Torr and (g)–(l) 100 mTorr oxygen at the indicated delay times from the arrival of the laser pulse. The 0.2 cm × 0.2 cm 248 nm laser pulse irradiated the YBCO target at the angle of 30° as shown.

A direct comparison of expansion into vacuum and 100 mTorr oxygen for delays following arrival of the laser pulse at $\Delta t = 0.5$–5.0 μs is given in Figs. 2(a)–2(f) and 2(g)–2(l) respectively. In 100 mTorr oxygen, the plume expansion dynamics are virtually indistinguishable from that in vacuum for $\Delta t < 1.0$ μs (Fig. 2(g)) with the plume again separating into nearly stationary and $v_{le} \approx 1.0$ cm μs^{-1} components. However, at $\Delta t = 1.0$ μs, a third component of the plasma emission appears on the leading edge of the expanding plasma as a sharp contact front of greater radius of curvature (Fig. 2(h)). A comparison of the vacuum and 100 mTorr plasma emission intensity contours at $\Delta t = 1.0$ μs (from Figs. 2(b) and 2(h)) is given in Fig. 4. The sharp frontal boundary which appears at $\Delta t = 1.0$ μs is highly suggestive of a shock front.

From $\Delta t = 1.0$–2.0 μs, the emission becomes dominated by that at the expansion front as the propagating two-component plume fluorescence coalesces into a common front which becomes considerably slowed (Fig. 2(i)) compared with the vacuum case (Fig. 2(c)). The plume continues to slow behind this sharp front until nearly stopped ($v_{le} \approx 0.06$ cm μs^{-1} at $\Delta t = 8.0$ μs under these conditions).

Position–time R–t plots of the leading edge of the plasma emission (along the normal to the irradiated region) from ICCD images, including those of Fig. 2, are given in Fig. 5. In vacuum, the leading edge maintains a constant velocity of 1.0 cm μs^{-1}. In 100 mTorr oxygen, however, the plume appears unaffected by the background gas for the first microsecond and then slows progressively as shown. Two fits to the 100 mTorr

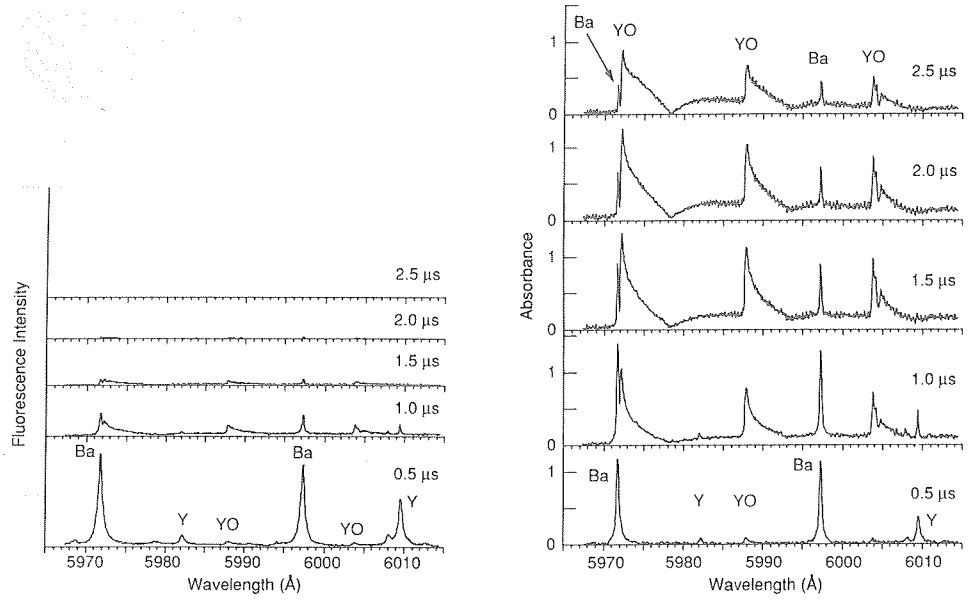

Fig. 3. Fluorescence and absorption of the laser-produced plasma at $d = 1$ mm from a YBCO pellet irradiated with 1.0 J cm^{-2} at 248 nm in 10^{-6} Torr. Spectra represent 200 accumulations with 20 ns temporal gate and 0.1 Å spectral resolution. While the fluorescence disappears by 2.5 μs, optical absorption reveals the presence of ground state species to much later times.

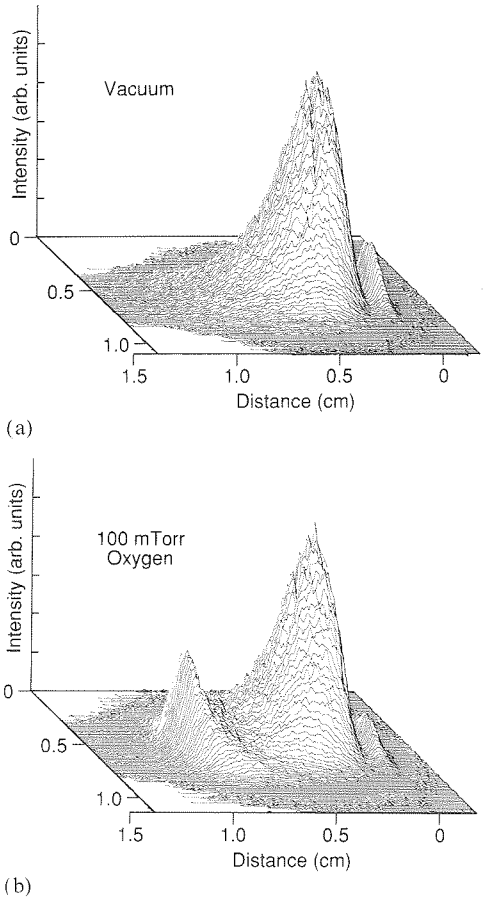

Fig. 4. Visible plasma emission intensity at $\Delta t = 1.0$ μs following 1.0 J cm^{-2} KrF laser ablation of YBCO in (a) 1×10^{-6} Torr and (b) 100 mTorr oxygen. These are intensity plots of the ICCD photographs of Figs. 2(b) and 2(h) illustrating the formation of an expansion front due to background gas collisions.

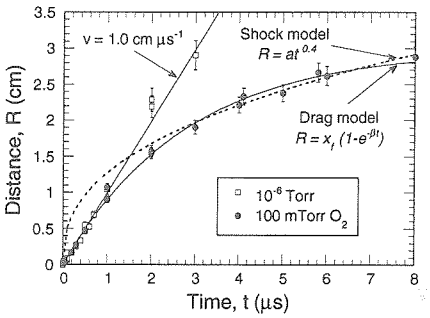

Fig. 5. R–t plots of the expansion front boundary of the luminous plume along the normal to the YBCO pellet measured from gated ICCD images including those of Fig. 2. Two fits to the 100 mTorr oxygen expansion data are shown: – – –, shock model $R = at^{0.4}$ with $a = 1.26$ cm μs$^{-0.4}$; ——, drag model $R = x_f[1 - \exp(-\beta t)]$ with $x_f = 3.0$ cm, $\beta = 0.36$ μs^{-1}. The error bars account only for uncertainties in estimating the position of the expansion front boundary.

data are given in Fig. 5: a shock model $R = at^{0.4}$ with $a = 1.26$ cm μs$^{-0.4}$ (broken line), and a drag model $R = x_f[1 - \exp(-\beta t)]$ with $x_f = 3.0$ cm, $\beta = 0.36$ μs^{-1} (full line). These models will be briefly discussed below.

For high background pressures a blast wave model [13, 14] has been used to describe the luminous shock front caused by the expansion of laser ablation plasmas [4]. This model was developed to describe the propagation of a shock wave through a background gas (density ρ_0) caused by the sudden release of energy E in an explosion. The propagation of the shock front by the background gas follows the distance–time relation $R = \xi_0(E/\rho_0)^{1/5}t^{2/5}$ where ξ_0 is a constant. This model strictly applies when the mass of the ejected products is

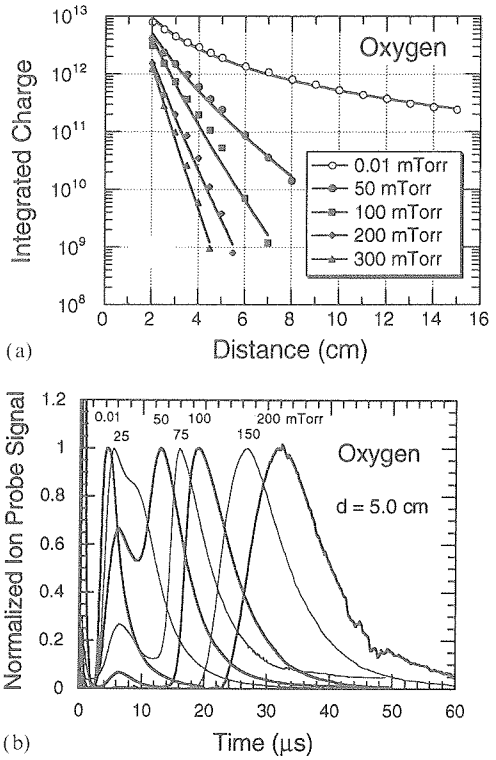

Fig. 6. (a) Integrated positive ion charge transmitted through oxygen backpressures of 0.01, 50, 100, 200, and 300 mTorr and measured by fast ion probe along the normal to a YBCO pellet irradiated with 3.0 J cm^{-2} 248 nm irradiation. Fits to the data are of the form $d^{-1.8}\exp(-bd)$ where b is the attenuation coefficient and d is the distance from the pellet. (b) Normalized ion probe current waveforms measured at $d = 5.0$ cm along the normal to a YBCO pellet irradiated with 3.0 J cm^{-2} 248 nm irradiation in 0.01, 25, 50, 75, 100, 150, and 200 mTorr oxygen.

small compared with the mass of the background gas set in motion by the shock [13], a situation which does not apply here.

At low pressures, such as those used for PLD, fits of the form $R = at^{0.4}$ to R–t plots like Fig. 5 consistently predict greater propagation distances than actually measured at early times. Fits of the form $R = at^n$ suggest exponents $n > 0.4$ ($n = 0.57$ for Fig. 5, not shown) [8] for limited improvement at early times. Ignoring the temporal region prior to the observed formation of the shock front, the blast wave model describes this phase of the expansion increasingly well at higher background pressures [4, 8, 9].

A classical drag force model (full line in Fig. 5) shows better agreement at low pressure and early times. The ejected pulse of ablation products is regarded as an ensemble which experiences a viscous force proportional to its velocity through the background gas. The equation of motion is $a = -\beta v$, giving

$$v = v_0 \exp(-\beta t) = v_0 - \beta x$$

$$x = x_f[1 - \exp(-\beta t)]$$

where β is the slowing coefficient and $x_f = v_0/\beta$ is the stopping distance of the plume.

The drag model predicts that the plume will eventually come to rest, as a result of resistance from collisions with the background gas, while the shock model (neglecting viscosity) predicts continued propagation $R \propto t^{0.4}$. Experimentally, the plume "range" is limited by attenuation more than slowing due to thermalization.

Figure 6 illustrates the combined attentuation and slowing of the laser plasma from ion probe measurements of the positive ion flux transmitted through background oxygen. The total integrated positive charge (measured by fast ion probe along the normal to a YBCO pellet irradiated with 3.0 J cm^{-2} 248 nm irradiation) transmitted *vs.* distance for various oxygen pressures is shown in Fig. 6(a). In vacuum, the ion flux drops as $d^{-1.8}$, in near agreement with the expected d^{-2} drop for a detector of constant size at distance d from the origin of the expansion. Using the vacuum density for I_0 the attenuation of the integrated charge was fitted to $I = aI_0 \exp(-bd)$, where $b = N\sigma$ represents the attenuation coefficient. The attenuation coefficient was found to depend linearly on background pressure where the slope of the curve yields a general scattering cross-section $\sigma_{i-O_2} = 2.3 \times 10^{-16}$ cm^2 for ion–oxygen interactions for background pressures up to 300 mTorr [7].

Figure 6(b) compares seven normalized ion probe current waveforms of the plasma arrival at $d = 5.0$ cm for ambient oxygen pressures from 0.01 to 200 mTorr. The integrated magnitudes of these waveforms dropped exponentially with pressure at a given distance (which can be inferred from Fig. 6(a)). Since the ion probe is a flux-sensitive detector ($F(t) = N(t)v(t)$) biased to collect positive ions, the waveforms of Fig. 6(b) are representative of the moving positive charge in the plume and not the stopped vapor.

At low pressures, the plasma displays a two-component character as in Figs. 2(g)–2(i): a fast component which is transmitted with little delay, and a component which has undergone pronounced slowing. As the background pressure is increased, more of the plume is delayed to longer times and a single-component pulse shape is acquired past about 100 mTorr.

Ion probe data give similar results. Figure 7 maps the propagation of the peak of the ion probe current pulse through ambient oxygen pressures of 50, 100, 200, and 300 mTorr along the normal to the pellet following 2.5 J cm^{-2} KrF irradation. While the overall fits to the data are better represented by the drag model, the plume is found to overshoot the predicted range and to continue propagating more like a shock wave. Fits of the same data to a shock-like power law model $R = at^n$ yielded values of the power law exponent varying from $n = 0.54$ at 50 mTorr to $n = 0.45$ at 300 mTorr, suggest-

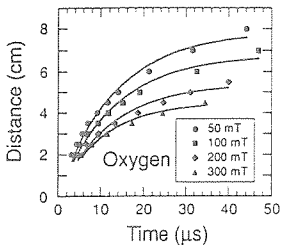

Fig. 7. Position–time plots of the plasma propagation through background oxygen following 2.5 J cm^{-2} KrF irradiation. Points represent arrival times of the peak of the positive ion flux from a Langmuir probe. Fits to the curves are of the form $R = x_f[1 - \exp(-\beta t)]$ where $x_f = 7.9$ cm, 6.8 cm, 5.4 cm, and 4.5 cm and $\beta^{-1} = 13.0$ μs, 12.9 μs, 12.1 μs, and 10.2 μs, for 50 mTorr, 100 mTorr, 200 mTorr, and 300 mTorr respectively.

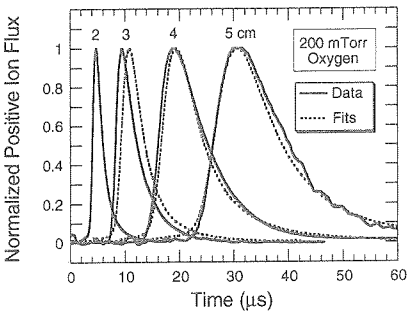

Fig. 8. Normalized ion probe waveforms (——) at 2, 3, 4, and 5 cm normal to a YBCO target irradiated with 2.5 J cm^{-2} at $\lambda = 248$ nm in 200 mTorr oxygen illustrating the delay and broadening of ion flux arrival times due to thermalization of the plume. – – –, ion fluxes simulated by propagating at 2 cm waveform to 3, 4, and 5 cm with a shock propagation model where the position evolves as $R = at^{0.49}$.

ing a better agreement with the $R = at^{0.4}$ shock model at higher pressures.

To investigate the validity of the shock propagation model following the transition region, ion probe waveforms were recorded at 2, 3, 4, and 5 cm following 2.5 J cm^{-2} ablation of YBCO in 200 mTorr oxygen and are shown in Fig. 8. The shape of the entire positive ion pulse arriving at 3, 4, and 5 cm was modeled on the basis of the 2 cm waveform and a generalized $R = at^n$ shock model. The data are the full curves in Fig. 8.

The ion probe current at a given time t results from the incident flux $N(t)v(t)$ at that moment, where $N(t)$ is the number density and $v(t)$ is the velocity. From the arrival times at $x = 2$ cm and the shock relation $v(x, t) = nx/t$, the number density and corresponding velocity $N_2(t)$ and $v_2(t)$ were separately determined according to the shock model. The arrival times and velocities of the 2 cm number density $N_2(t_2)$ were determined at subsequent distances by the relations $v_j = v_2(x_j/2)(t_2/t_j)$ where $t_j = t_2(j/2)^{1/n}$. The modeled flux $N_2(t_j)v_j$ downstream was then constructed for comparison with the measured current. The power law exponent n was iterated to determine the best fit to the 5 cm waveform. The results are shown by the broken lines in Fig. 8. The value of the best-fit exponent is $n = 0.49$.

Figure 8 demonstrates that the entire shape of the pulse of positive ions is well represented by a power law dependence shock propagation model for the higher background oxygen pressures in the film growth regime.

4. Conclusions

The propagation of the plume of KrF laser ablated material from a YBCO target into vacuum and ambient oxygen pressures used for film growth has been studied by fast ICCD photography, ion probe measurements, and high resolution optical emission and absorption spectroscopy. These four spatially and temporally resolved techniques are diagnostics which can be applied to high density laser plasmas in reactive ambient gas conditions, such as those used for growth of high T_c superconductor films. The combined measurements indicate that gas dynamic effects play a dominant role in the formation and propagation of the pulse of ejectants.

In vacuum, the initial plasma at the pellet surface separates into a nearly stationary section within 1 mm of the pellet surface and an expanding component which initially undergoes a one-dimensional expansion in vacuum and background gases for a given distance, followed by a three-dimensional free expansion in vacuum. Optical absorption spectroscopy reveals high densities of non-emitting neutrals and molecules at times much greater than the plume fluoresence in the "stationary" region, implying slowly moving, stopped or negative-going species resulting from collisions in the dense initial expansion region near the pellet.

In ambient gases, the expanding visible plasma plume undergoes a transition in space and time during the formation of a shock front. During this transition region, the plasma appears to have two components, an initial fast component which has traveled at nearly vacuum speed and a delayed component. Ion probe waveforms show these two components and the disappearance of the fast components as the shock front consolidates.

At the lower pressures investigated here, the propagation of the plume agrees with a drag model during the initial expansion, when the mass and pressure of the plume material are greater than that of the gas with which it has interacted. This model predicts the eventual stopping of the plume due to a viscous drag force.

This expansion front contains the ablation products, in contrast to the blast wave model which follows a shock wave disturbance through the gas itself. The power law dependence form of the shock propagation model, however, appears to describe the propagation of this

expansion front and, in fact, the shape of the entire positive ion waveform. The value of the power law exponent $n = 0.49$ for 200 mTorr oxygen, is greater than that predicted by blast wave theory.

Fast ion probes sensitive to the flux of positive ions reveal that the ions are attenuated exponentially with distance and pressure, in accordance with a simple scattering model which yields an oveall ion–oxygen reaction cross-section $\sigma_{i-O_2} = 2.3 \times 10^{-16}\,cm^2$ for oxygen pressures up to 300 mTorr.

Acknowledgments

The author gratefully acknowledges the technical expertise and assistance of Yair Talmi, Hollis Davis and Chris Meyers of Princeton Instruments Inc. as well as the loan of the gated ICCD camera. The photographic advice of Jim Richmond also is appreciated. This work was supported by the Division of Materials Sciences, US Department of Energy, under Contract DE-AC05-84OR21400 with Martin Marietta Energy Systems, Inc.

References

1 T. Venkatesan, *et al.*, *Appl. Phys. Lett.*, *53* (1988) 1431.
2 J. P. Zheng, Q. Y. Ying, S. Witanachchi, Z. Q. Huang, D. T. Shaw and H. S. Kwok, *Appl. Phys. Lett.*, *54* (1989) 954.
3 C. Girault, D. Damiani, J. Aubreton and A. Catherinot, *Appl. Phys. Lett.*, *55* (1989) 182.
4 P. E. Dyer, A. Issa and P. H. Key, *Appl. Surf. Sci.*, *46* (1990) 89. P. E. Dyer, A. Issa and P. H. Key, *Appl. Phys. Lett.*, *57* (1990) 186.
5 A. Gupta, B. W. Hussey, A. Kussmaul and A. Segmuller, *Appl. Phys. Lett.*, *57* (1990) 2365.
6 K. Scott, J. M. Huntley, W. A. Phillips, J. Clarke and J. E. Field, *Appl. Phys. Lett.*, *57* (1990) 922.
7 D. B. Geohegan, in *Surface Chemistry and Beam–Solid Interactions*, Materials Research Society, Pittsburgh, PA, 1990, p. 557.
8 D. B. Geohegan, in *Laser Ablation—Mechanisms and Applications*, Springer, Berlin, 1991, p. 28.
9 D. B. Geohegan, in E. Fogarassy and S. Lazare (eds.), *Laser Ablation of Electronic Materials: Basic Mechanisms and Applications*, Elsevier, Amsterdam, 1992, p. 73.
10 R. Kelly and B. Braren, *Appl. Phys. B*, *53* (1991) 160.
11 R. Kelly, *J. Chem. Phys.*, *92* (1990) 5047, and references cited therein.
12 R. M. Gilgenbach and P. L. G. Ventzek, *Appl. Phys. Lett.*, *58* (1991) 1597.
13 Ya. B. Zel'dovich and Yu. P. Raizer, in *Physics of Shock Waves and High Temperature Hydrodynamic Phenomena*, Vol. 1, Academic Press, New York, 1966, p. 94.
14 M. A. Liberman and A. L. Velikovich, in *Physics of Shock Waves in Gases and Plasmas*, Springer, Berlin, 1986.
15 H. W. Liepmann and A. Roshko, *Elements of Gasdynamics*, Wiley, New York, 1957.
16 D. B. Geohegan and D. N. Mashburn, *Appl. Phys. Lett.*, *55* (1989) 2345.
17 D. B. Geohegan, *Appl. Phys. Lett.*, *60* (1992) 2732.